A SMA-based actuation system for a fish robot

Chan Hoang Le, Quang Sang Nguyen and Hoon Cheol Park*

Department of Advanced Technology Fusion, Konkuk University, Seoul 143-701, Korea

Abstract.   We design and test a shape memory alloy (SMA)-based actuation system that can be used to propel a fish robot. The actuator in the system is composed of a 0.1 mm diameter SMA wire, a 0.5 mm-thick glass/epoxy composite strip, and a fixture frame. The SMA wire is installed in a pre-bent composite strip that provides initial tension to the SMA wire. The actuator can produce a blocking force of about 200 gram force (gf) and displacement of 3.5 mm at the center of the glass/epoxy strip for an 8 V application. The bending motion of the actuator is converted into the tail-beat motion of a fish robot through a linkage system. The fish robot is evaluated by measuring the tail-beat angle, swimming speed, and thrust produced by the tail-beat motion. The tail-beat angle is about 20°, the maximum swimming speed is about 1.6 cm/s, and the measured average thrust is about 0.4 gf when the fish robot is operated at 0.9 Hz.

Keywords: fish robot; SMA wire; bending actuator; biomimetics

1. Introduction

Electromagnetic motors have been widely used for robotic systems for many decades. Motors typically produce rotary motion that needs to be transformed into linear and/or angular motion through a complex linkage mechanism in a robotic system. This is why a robotic system is typically large, and is hard to reduce in size. So-called artificial muscles are actuators that can be electrically activated to provide linear deformation, just like real muscles. Because of this feature, an artificial muscle-based actuation mechanism can be compact for use in a miniaturized robotic system. Another advantage over conventional electromagnetic motors is low noise and less electromechanical signature, which allows the development of stealthy robots. Ionic polymer-metal composites (IPMCs) (Shahinpoor *et al*. 2004), piezoceramic materials (Crawley and Javier 1987), and shape memory alloy (SMA) wires (Duerig *et al*. 1990), are the most widely used artificial muscle actuators in the new class of underwater robotic systems.

An IPMC can produce a large bending deformation for a 2 to 3 V application in wet conditions. Thus, IPMCs are potentially suitable for actuation systems of swimming robots. Nakadoi *et al.* presented a small-scale fish-like robot, propelled by an IPMC actuator that was intended to swim in blood vessels (Nakadoi *et al.* 2008). However, the actuation force produced by an IPMC actuator is typically small, and the device may not produce enough thrust force. For a higher actuation force, we need to apply higher voltage and current to an IPMC, or use multiple IPMC actuators. For example, sixteen IPMC strips were used for two pectoral fins in a ray-like robot (Punning *et al*. 2004).

Another choice for a relatively large actuation force is a piezoceramic material-based actuator.

Piezoceramic materials have been widely used for sensors and actuators due to their relatively fast response. However, their actuation displacements are much smaller than those of IPMCs. To overcome this limitation, bending-type unimorph actuators such as Thin Layer Unimorph Ferroelectric Driver and Sensor (THUNDER) (Hellbaum *et al.* 1997) and Lightweight Piezo-Composite Actuator (LIPCA) (Yoon *et al.* 2004) have been developed in an effort to amplify bending displacement. However, such increased actuation displacement is still too small to produce a large tail-beat angle for an underwater system. Therefore, another angle amplification mechanism should be devised for a successful swimmer. Two THUNDER actuators were used in the actuation system of a floating boat in which an angle amplification mechanism was implemented (Borgen *et al.* 2003). A series of fish robots have been developed by using two parallel LIPCAs (Tedy *et al.* 2009) and four stacked LIPCAs (Nguyen *et al.* 2009). However, THUNDER and LIPCA can produce only limited actuation forces.

From the viewpoint of actuation force, SMAs can be the best choice. SMAs can produce large actuation forces and acceptable displacement. In recent research, SMA wires have been used for propulsion systems of fish robots. An example of a relatively large-scale tuna fish robot has been reported (Suleman and Crawford 2008). The tuna robot operated at 0.5 Hz with a power consumption of about 333.6 W. Even though the fish robot required high power, its tail beat frequency was relative low. In studies of small fish robots, two SMA wires were embedded on both sides of a plastic substrate to create the tail-beat motion (Wang *et al.* 2008, Wang and Hang 2008). In these models, the SMA wires were in contact with water through a thin skin layer to cool the SMA wires after actuation. In this case, the tail-beat frequency of the fish robot could be increased, but more power consumption would be expected.

Despite the high force production capability of SMAs, researchers have been hesitant to use SMAs because they show relatively slow response and limited actuation displacement--typically less than 4% strain. To overcome these disadvantages, a new approach is required. SMA-based actuation mechanisms with additional springs could be used to provide recovery force immediately after actuation of the SMA wires. As a potential fish robot mechanism, a hydrofoil system with combination of multiple linear spring and SMA wires was introduced. The hydrofoil could deform the whole body as desired due to the actuation force provided by the SMA wires, which may mimic carangiform fish locomotion (Rediniotis *et al.* 2002). In another fish robot mechanism, instead of linear springs, a bendable elastic structure was used in (Rossi *et al.* 2011) as anchoring and tension regulating mechanism. However, no further detail on the elastic structure was provided in the reference.

With such designs, the devices can be repeatedly actuated at a reasonable frequency. However, the actuation displacement might be reduced in this case, and the devices would be complex or large in size, which is not plausible for miniaturized robots. Recently, a small crawling robot was successfully demonstrated with an acceptable walking frequency of 3 Hz (Aaron *et al.* 2008). In this robot, relatively long SMA wires were installed around flexible robot frames. The SMA wires bent the elastic frames during actuation or contraction, and the bending energy stored in the frames during actuation was released for quick recovery of the SMA wires to their original length. Thus, actuation displacement and response speed were improved at the same time. As an effort to improve actuation response of SMA actuators through an electric power control, Featherstone *et al.* demonstrated a way of current control by measuring current and electric resistance of an SMA element (Featherstone *et al.* 2004).

In this work, we present an SMA wire-based bending actuator. The bending actuator is composed of an SMA wire connected to a pre-bent glass/epoxy strip and fixture frame. The force used to

initially bend the strip provides the initial stress in the SMA wire. An additional bending of the composite strip is created due to the contraction of the SMA wire when heated, which is used to create tail-beat motions in one direction. The elastic energy stored in the glass/epoxy strip during the heating phase of the SMA wire is released in the cooling phase. The released elastic energy forces the SMA wire return to its initial length even before it is fully cooled down and creates tail-beat motions in the reversed direction. The bending actuator actually amplifies the actuation displacement of the SMA wire in this mechanism. Thus, both the actuation displacement and response speed were improved at the same time. The bending actuator was installed in a waterproof body of a fish robot to create tail-beat motion. In the actuation system of the fish robot, the displacement at the center of the glass/epoxy strip was converted to tail-beat motion of the fish robot through a linkage system. We have assumed that an installed battery is used for the actuation system and no power control is applied to operate the fish robot. Instead, we have applied a certain level of power to the installed SMA wire, so that we can use the SMA wire without damage. In the following sections, the design and testing of the bending actuator are described in detail. We also describe the measured tail-beat angle, swimming speed, and thrust force of the fish robot.

2. SMA wire-based bending actuator

2.1 Actuator design

The bending actuator consists of an SMA wire (Flexinol 0.1 mm, Dynalloy Inc., USA, T_{As}=70°C, Technical Characteristics of Flexinol® Actuator Wires, www.dyalloy.com), a glass/epoxy strip, and an acrylic fixture frame. The glass/epoxy (GE) strip is made of glass/epoxy prepreg (GEP108, SK Chemical, Korea). Depending on the number of prepregs, the thickness of the GE strip may vary. The GE strip plays an important role in the bending actuator by storing and releasing bending energy during the heating and cooling phases of the SMA wire, respectively. Moreover, the bending motion at the center of the GE strip is transformed to the tail-beat motion of a fish robot through a specially-designed linkage system. The most important part of the actuator system is the SMA wire. In this study, 0.1 mm diameter SMA wire was used. The SMA wire was connected to a pre-bent GE strip and fixture frame. Thus, the SMA wire was always under tensile stress.

The level of the applied tensile stress depends on the thickness and the curvature of the GE strip. In SMA wire, the initial tensile stress has a strong effect on the strain production. Therefore, the thickness and curvature of the GE strip should be carefully considered so that a recommended initial tensile stress can be prescribed. Based on our experiment, the maximum loading applied to the SMA wire should be from 500 MPa to 600 MPa because for tensile stress higher than 600 MPa, the SMA wire is stretched below the detwinned martensite length. In this study, the diameter of the

Table 1 Dimensions of GE strip and SMA wire

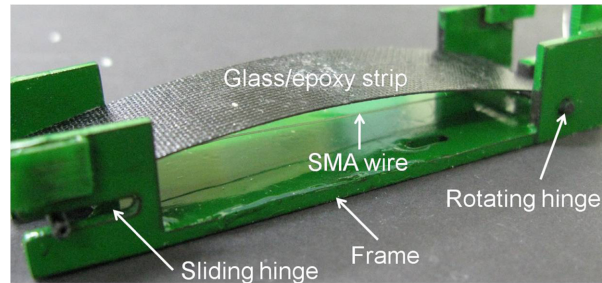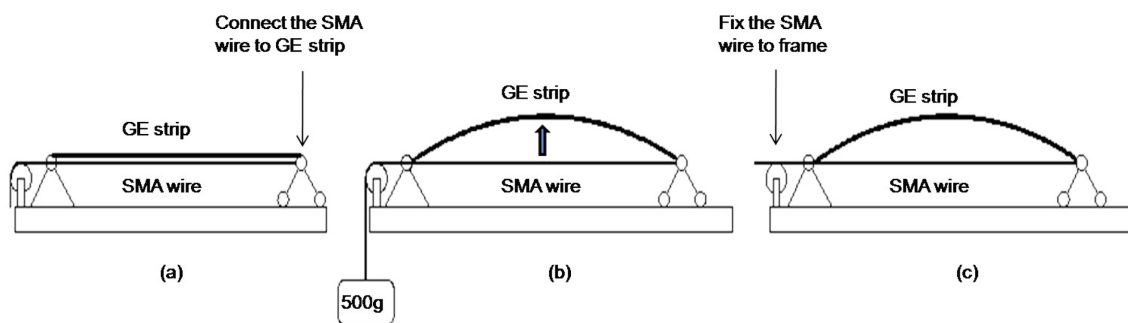| GE strip		SMA wire	
Dimensions	70 mm × 20 mm	Diameter	0.1 mm
Thickness	5 layers: 0.424 mm	Length	< 70 mm
	6 layers: 0.496 mm		
	7 layers: 0.574 mm		

Fig. 1 Bending actuator

Fig. 2 Installation of SMA wire in the GE strip and frame. (a) SMA wire and GE strip connected at the sliding hinge, (b) a dummy weight is connected to the SMA wire, and the GE strip is bent, and (c) the SMA wire is fixed to the frame and the dummy weight is removed

SMA wire was 0.1 mm. Therefore, the load applied to the SMA wire should not be greater than about 500 gf. In order to create the maximum recovery force, a load of 500 gf was used as the initial tension applied to the SMA wire. Table 1 describes the GE strip and the SMA wire.

The acrylic frame holds the bent GE strip and installs the SMA wire, and delivers actuation displacement and force to a linkage system. One end of the GE strip allows rotational motion, and the other end can move in the horizontal direction in a slot in the frame. Fig. 1 shows a photo of the bending actuator.

Fig. 2 shows how the SMA wire was installed on the frame and the GE strip. The SMA wire was fixed at the sliding hinge (right end), and initial tension was applied at the left end of the SMA wire by attaching a dummy weight. The SMA wire was fixed at the frame while the initial tension was applied. After the SMA installation, the dummy weight was removed. The applied initial tension was 500 gf. During this process, the GE strip had a reasonable curvature and height at the center, and continued to apply the initial tension even after removal of the dummy weight.

2.2 Selection of GE strip

The GE strip applies an initial tension to the SMA wire as a reaction force developed during the SMA installation. Actuation of the installed SMA wire by heating, which is contraction in this case, produces additional curvature in the GE strip. The SMA wire starts to recover its original length immediately after the heating phase, and the additionally deformed GE strip returns to the initially bent shape. If the force induced by the additionally deformed GE strip is large enough, then the
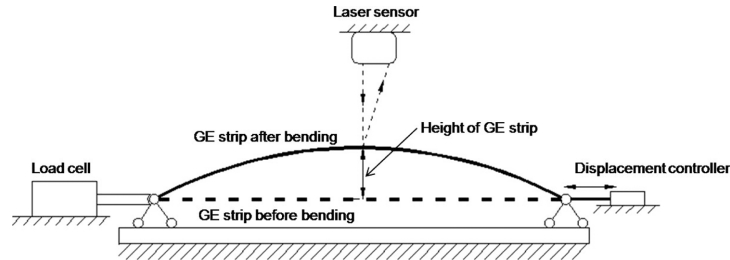
Fig. 3 Reaction force measurement

SMA wire can recover its own length more quickly. Thus, if the stiffness of the GE strip is properly chosen, an actuator can be designed such that it creates a relatively large actuation force and displacement, and works at a higher frequency.

We measured the reaction forces of three candidate GE strips with different thickness, as listed in Table 1. The reaction force of a strip provides tensile force after an SMA wire is installed into the pre-bent strip. Fig. 3 shows the experimental setup used for the reaction force measurement. In this experiment, a load cell (333FB, Ktoyo, Korea) was attached to one end of a strip. The load cell measured the reaction force at the left end, as shown in Fig. 3. The other end of the strip was connected to a displacement controller (DC-3KS, Marzhauser, Germany). The right end of the GE strip was pushed to the left hand side using the displacement controller. A laser sensor (LKG85, Keyence, Japan) was used to measure the height of the center of the GE strip. The reaction force measured at the left end of the GE strip was equivalent to the tensile force to be applied in the SMA wire after the SMA wire is installed in the GE strip.

Next, we measured the recovery force of the three GE strips. The recovery force is produced by a GE strip during recovery of the strip after additional bending due to actuation of an installed SMA wire. The recovery force is used to quickly recover the initial length of the SMA wire after actuation. When the actuator is assembled with a linkage system, the recovery force is used to create a tail-beat motion in the reverse direction immediately after an initial tail-beat motion is created by contraction of the SMA wire during the heating phase. This will be described in more detail in Section 2.3. Fig. 4 shows our experimental setup for the recovery force measurement.

As in the reaction force measurement, a displacement controller was used to control the displacement applied to the GE strip. In this way, we controlled the height of the GE strip center. At each given height of the GE strip, the load cell was connected to the strip. Then, we removed the applied displacement and measured the force produced by the bending down motion of the GE strip. The experiment was conducted for various heights of the three GE strips.
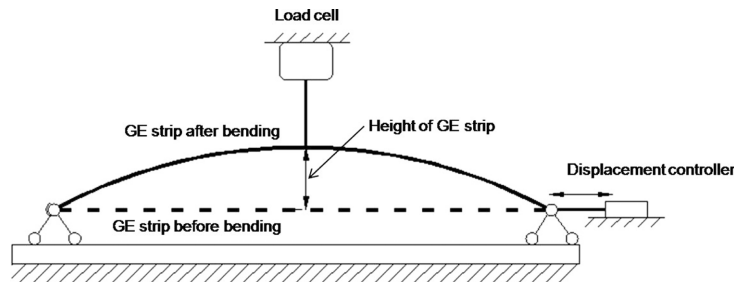

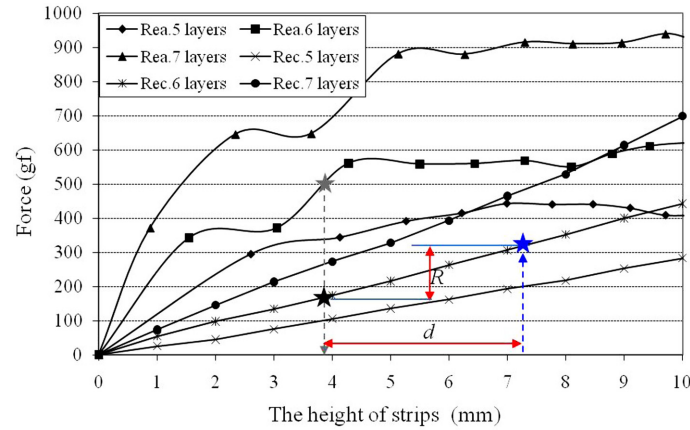Fig. 4 Recovery force measurement

Fig. 5 Recovery forces and reaction forces of various glass/epoxy layers. "Rea.5 layers" is the reaction force of a five-layer strip, "Rec.5 layers" is the recovery force of a five-layer strip, etc

Fig. 5 shows the measured reaction force and recovery force for three different GE strips. This figure shows that the six-layer GE strip produced a reaction force slightly lower than 600 gf with a reasonable height. Thus, the six-layer GE strip provided an appropriate tensile stress (about 500 MPa, shown by a grey star in Fig. 5) to an SMA for a height of about 3.8 mm. At this height, the six-layer strip produced a recovery force of about 160 gf, which is shown with a black star in Fig. 5. For an actuator composed of a six-layer GE strip, the strip can provide an appropriate initial tension of 500 gf to the installed SMA wire for an initial height of 3.8 mm. In this configuration, when electric power applied to heat the SMA wire to T_{As} triggers contraction, the GE strip can create additional height or actuation displacement. For example, for an 8 V application, the actuation displacement can be 3.5 mm (denoted by d in Fig. 5), which will be considered in Section 3. In this case, the GE strip can create a recovery force of about 320 gf (denoted by a blue star on the right side in Fig. 5). However, the strip maintained the initial height of 3.8 mm even after the SMA wire cooled down, and the useful recovery force provided by the strip could be about 160 gf, which is shown by R in Fig. 5. This force is used to create tail-beat motions in the reverse direction after the actuator creates the initial tail-beat motion by using actuation force or blocking force, as described in Section 2.3.

2.3 Measurement of blocking force

Based on the aforementioned results, a GE strip with six layers and a reaction force of 500 gf was selected for the bending actuator. To confirm that the actuator under an initial tension of 500 gf could create a large actuation force, the blocking force of the bending actuators with a six-layer strip was measured under different initial tensions. To measure the blocking force of the bending actuator, we designed the experimental setup shown in Fig. 6. The experiment was carried out after applying different initial tensile stress levels to an SMA wire. Then, the blocking forces were measured for an 8 V input and a heating time of 0.25 s.

Fig. 7 shows the measured blocking forces of the actuator with the six-layer strip under various initial tensions from 100 gf to 500 gf. We note that the maximum blocking force is about 200 gf for an initial tension of 500 gf. Also, the blocking force reached its maximum value quickly during the
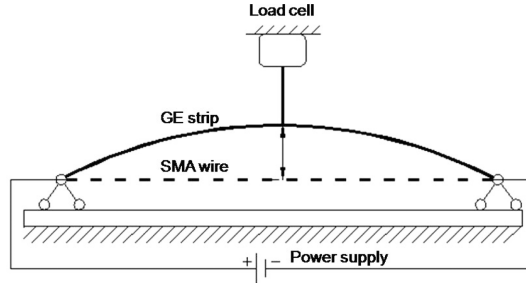
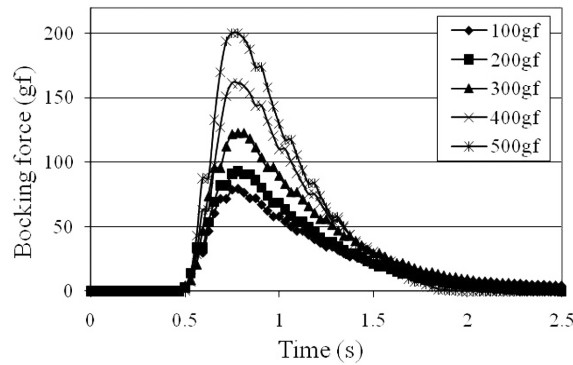Fig. 6 Experiment setup for blocking force measurement

Fig. 7 Blocking forces of the bending actuator for different initial tensions

heating time of 0.25 s. However, recovery of the SMA wire to its original length took more time due to a slightly lower recovery force (160 gf) as explained in Section 2.2, and to the presence of the SMA wire.

2.4 Determination of the heating time and frequency

As the final step in the actuator design, we determined the heating time for the SMA wire, and the excitation frequency of the actuator. Because we have not intended to control power in this study, we applied power to the SMA wire with voltage control and did not measure the corresponding current. Since the linear resistance of the SMA wire is given as 3 Ω/in (or 1.18 Ω/cm) in the specification, we can estimate the current, even though the resistance can vary due to the temperature change. A rectangular-wave-form input voltage was used to quickly raise temperature in the SMA wire.

Fig. 8 shows the measured actuation displacement of the bending actuator under an 8 V input at a 0.5 Hz excitation frequency for various heating times. We have chosen 8 V through multiple tests, and we have found that the actuation performance is not noticeably degraded after repeated actuations for this condition. For a longer term use, we may lower the power level. Even in this case, we can follow the design process suggested in this work to investigate characteristics of the actuation system. We note that the maximum displacements were almost the same (3.5 mm) for heating times from 0.25 s to 0.4 s. In order to assign more time for cooling of the SMA wire after actuation, the heating time of the SMA wire should be reduced as much as possible. Therefore, 0.25 s was selected as the heating time of the SMA wire. Similarly, Fig. 9 shows that the maximum blocking
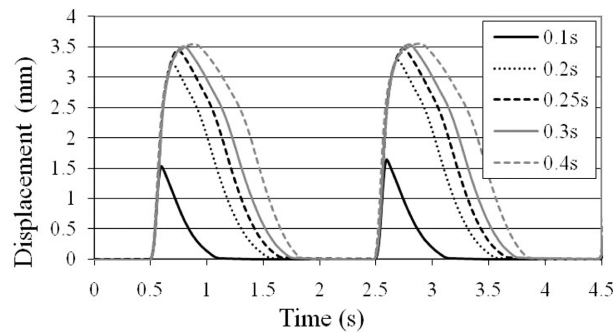
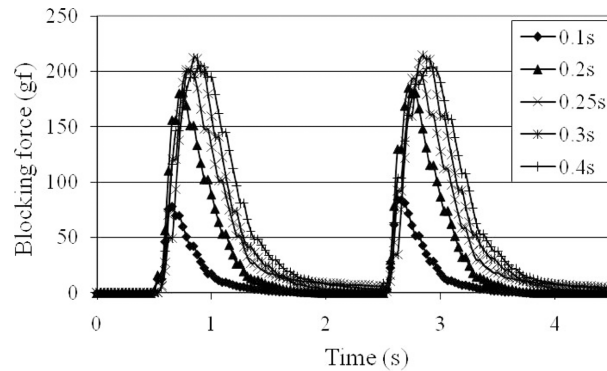Fig. 8 Displacement of bending actuator for 8 V at 0.5 Hz

Fig. 9 Blocking force of bending actuator for 8 V at 0.5 Hz

forces were similar for heating times of 0.25 s to 0.4 s. Thus, for an 8 V input with a heating time of 0.25 s, Figs. 8 and 9 show that the actuator can create an actuation displacement of 3.5 mm and a blocking force of 200 gf at the center of the GE strip. During operation, due to this actuation, the height of the center of the GE strip was changed from 3.8 mm (the original height) to 7.3 mm. From Fig. 5, we note that the recovery force was about 160 gf, which is 320 gf to 160 gf (*R* in Fig. 5) for this height change. Therefore, a blocking force of 200 gf and a recovery force of 160 gf will be generated due to the actuation of the SMA wire and recovery of the GE strip, respectively. The difference is about 20%.

For actuation at 0.5 Hz with a heating time of 0.25 s, the displacement and blocking force return to zero after turning off the power to the SMA wire. In other words, the GE strip and the SMA wire return to their initial shapes. This means that the SMA wire is ready for the next actuation after enough cooling time. Therefore, we can slightly increase the frequency by reducing the cooling time of the SMA wire.

Figs. 10 and 11 show the measured displacement and blocking force, respectively, for a repeated actuation at 0.75 Hz with the same heating time. The maximum displacement and blocking force are almost the same as those shown in Figs. 8 and 9 for 0.5 Hz, respectively. The SMA wire still recovered its initial length after a 0.25 s actuation before the next actuation. Therefore, we chose this condition for the actuator to propel the fish robot.
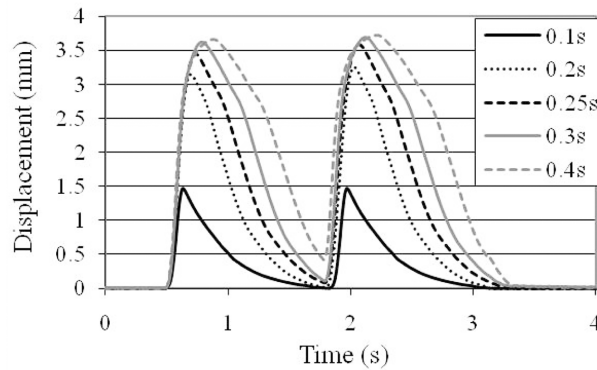
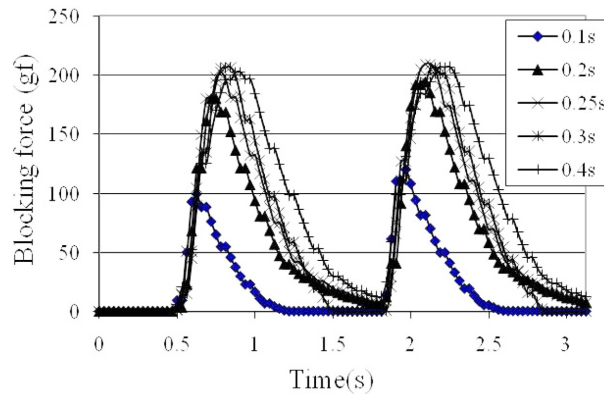Fig. 10 Displacement of bending actuator for 8 V at 0.75 Hz

Fig. 11 Blocking force of bending actuator for 8 V at 0.75 Hz

3. Fish robot assembly

3.1 The linkage system

The size and actuation displacement range of the actuator are quite similar to those of the LIPCA (Wiguna *et al.* 2009), which is a piezoceramic unimorph actuator. Therefore, we used a similar linkage system and waterproof body used in a fish robot actuated by four LIPCAs (Nguyen *et al.* 2009). A conceptual drawing for the actuation system is included in Fig. 12(a). In the actuation system, an initially bent glass/epoxy strip provides an initial tension to the connected SMA wire and the recovery force. The linkage system, which is assembled above the composite strip, is designed to transform the limited bending actuation displacement of the actuator into a large tail-beat angle. Figs. 12(b) and (c) show how the tail beat motions are created when the electric power is applied to the SMA wire and when the power is turned off, respectively. A related video can be found at "www.youtube.com/watch?v=3Tj8AxakcI8&feature =youtu.be." More details of the kinematics analysis of the linkage system can be found in Nguyen *et al.* (2009). Fig. 12(d) shows the actual assembly of the actuation system and Fig. 12(e) displays the final assembly of the fish robot.
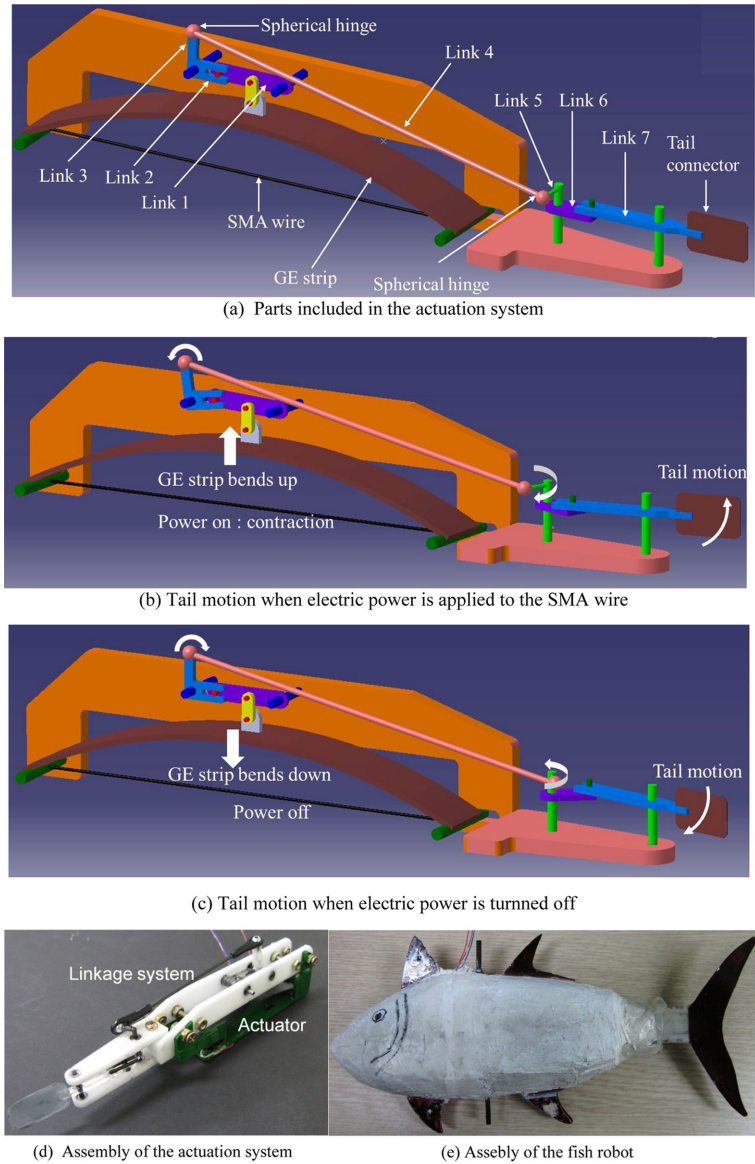
(a) Parts included in the actuation system

(b) Tail motion when electric power is applied to the SMA wire

(c) Tail motion when electric power is turnned off

(d) Assembly of the actuation system　　　　　(e) Assebly of the fish robot

Fig. 12 Assembly of fish robot

3.2 Final assembly of fish robot

The actuation system composed of the linkage and actuator was installed in the waterproof body. The body of the fish robot was made of acrylic and silicon materials. The fish robot has three main parts: SMA-based bending actuators, a linkage system, and a waterproof body. The final assembly is shown in Fig. 12(c). The dimensions of the fish robot are 26 cm long, 12.3 cm high, and 4 cm wide. We used an ostraciiform tail fin (Sfakiotakis *et al.* 1999) with an area of 16.8 cm^2.

4. Evaluation

4.1 Measurement of tail-beat angle

To measure the tail-beat angle in water, the fish robot was clamped in a fixture and placed in a water tank. The width of the water tank was about 180 cm in diameter, which is large enough to avoid the wall effect. As the actuation system of the fish robot was excited, the tail-beat motions were captured by a high-speed camera (APX 120K, Photron Fastcam-Ultima, Japan). Time histories of the tail-beat angle in water were constructed based on the video images. The experimental setup is shown in Fig. 13.

4.2 Measurement of thrust force

The experimental setup for the thrust measurement is shown in Fig. 14. In this experiment, a load cell (Nano 17 Transducer, ATI Industrial Automation, USA) was used to measure the thrust generated by the fish robot. The diameter of the water tank was 180 cm, which is large enough to allow us to neglect the wall effect.
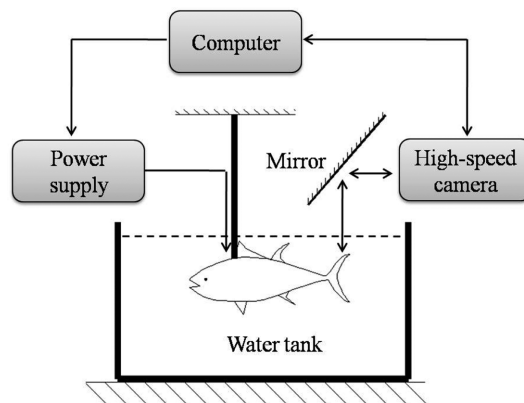

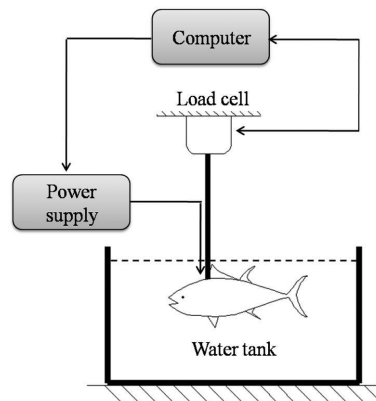Fig. 13 Experiment setup of tail-beat angle measurement

Fig. 14 Thrust force measurement

4.3 Swimming test

A swimming test was conducted inside the same water tank with a 30 cm water level. The acceleration distance was about 20 cm. After the fish robot swam for the acceleration distance, the time spent for swimming over the additional 80 cm distance was measured. From the given distance and measured time, we calculated the average velocity.

4.4 Experimental results

Fig. 15 shows the time history of the tail-beat angle at 0.75 Hz for an 8 V application. The tail-beat angle was about 24°. We note that the tail can return to the initial position and wait for a moment before starting a new tail-beat period. This might be caused by clearance among connections in the linkage and a relatively longer cooling time. Thus, if we eliminated the waiting time by reducing the cooling time, then the frequency could be slightly increased.

For the same heating time of 0.25 s, after we slightly reduced the cooling time, the frequency could be increased to 0.9 Hz. Figure 16 shows the time history of a tail-beat angle at 0.9 Hz. In this case, while slightly faster tail-beat motions could be achieved, the tail-beat angle was reduced to 20°. As shown in Figs. 8 to 11, we could not further reduce the heating time from 0.25 s for an 8 V application. Therefore, the maximum tail-beat frequency of the fish robot is 0.9 Hz.

Fig. 17 shows the measured average thrust at different frequencies. The average thrust increased as the tail-beat frequency was raised. The maximum thrust was about 0.4 gf at 0.9 Hz. The time
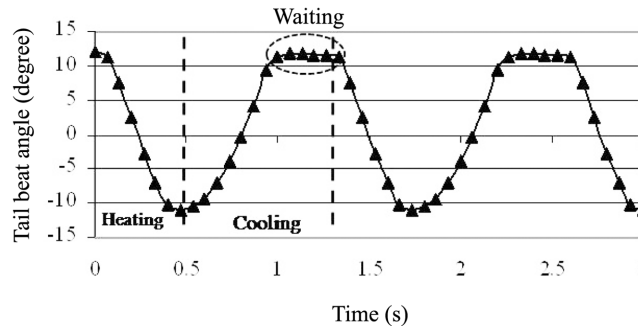

Fig. 15 Tail-beat angle at 0.75 Hz, 8 V, and 0.25 s of heating time
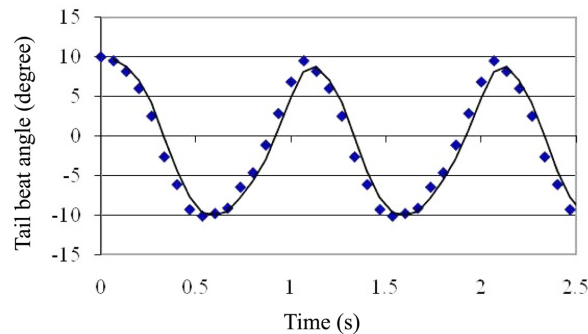

Fig. 16 Tail-beat angle at 0.9 Hz for an 8 V application with a heating time of 0.25 s
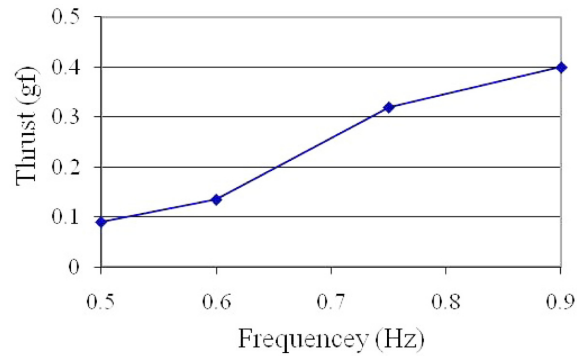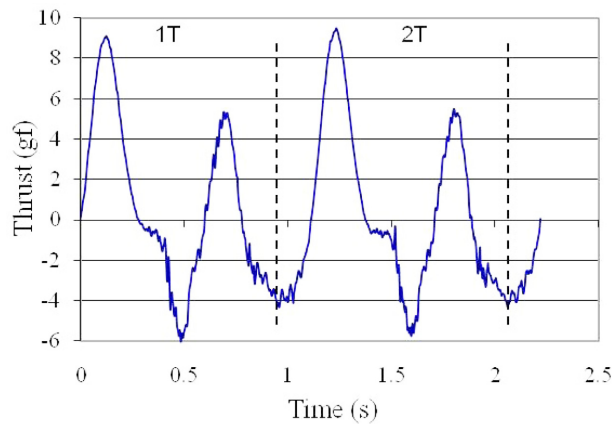
Fig. 17 Average thrust versus frequency

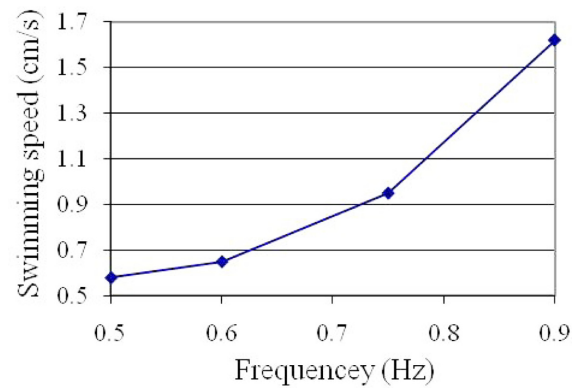Fig. 18 Time history of thrust for two periods at 0.9 Hz

Fig. 19 Swimming speed of the fish robot versus frequency

history of thrust in two periods of tail-beat motion is shown in Fig. 18. We note that the two peak thrusts in one period were not equal to each other. The peak thrusts produced by contraction of the SMA wire in the heating phase were larger than the peak thrust produced by the recovery of the GE strip during the cooling phase. This is mainly due to the difference in the blocking force (200 gf)

and recovery force (160 gf), as previously explained. The measured swimming speed of the fish robot at various frequencies is shown in Fig. 19. Swimming speed increased for a higher tail-beat frequency. The maximum speed reached about 1.6 cm/s at 0.9 Hz. Since the swimming distance was relatively short, the fish robot could swim almost straight despite the asymmetry of the two peak thrusts.

5. Conclusions

We proposed a detailed procedure for the construction of an SMA-based bending actuator. The actuator consists of an SMA wire, a glass/epoxy strip, and a frame. The best working conditions for the actuator were chosen from a series of measurements: reaction forces and recovery forces of the glass/epoxy strip, and the displacement and blocking forces of a bending actuator. The SMA bending actuator was assembled with a linkage system to transform the actuation displacement into tail-beat motion. The actuation system was installed in a fish robot body. The tail-beat angle, thrust force, and swimming speed of the fish robot were measured. The maximum speed of fish robot was 1.6 cm/s at 0.9 Hz. Despite a relatively slow swimming speed, this work shows the potential application of an SMA actuator to a fish robot.

Acknowledgements

References

Aaron, M., Hoover, E.S. and Ronald, S.F. (2008), "RoACH: An autonomous 2.4g crawling hexapod robot", *Proceedings of the IEEE/RSJ International Conference on Intelligent Robots and Systems*, Nice, France, September.

Borgen, M.G., Washington, G.N. and Kinzel, G.L. (2003), "Design and evolution of a piezoelectrically actuated miniature swimming vehicles", *IEEE-ASME T. Mech.*, **8**(1), 66-77.

Crawley, E.F. and Javier, D.L. (1987), "Use of piezoelectric actuators as elements of intelligent structures", *AIAA J.*, **25**(10), 1373-1384.

Duerig, T.W., Melton, K.N., Stockel, D. and Waymanm, C.M. (1990), *Engineering Aspects of Shape Memory Alloys*, Butterworth-Heinmann Ltd, London.

Featherstone, R. and Teh, Y.H. (2004), "Improving the speed of shape memory alloy actuators by faster electrical heating", *Proceedings of the International Symposium on Experimental Robotics*, Singapore, June.

Hellbaum, R.F., Bryant, R.G. and Fox, R.L. (1997), *Thin layer composite unimorph ferroelectric driver and sensor*, US Patent Specification 5632841.

Nakadoi, H., Sobey, D., Yamakita, M. and Mukai, T. (2008), "Liquid environment-adaptive IPMC fish-like robot using extremum seeking feedback", *Proceedings of the IEEE/RSJ International Conference on Intelligent Robots and Systems*, Nice, France, September.

Nguyen, Q.S., Heo, S., Park, H.C., Goo, N.S., Kang, T. and Yoon, K.J. (2009), "A fish robot driven by piezoceramic actuators and miniaturized power supply", *Int. J. Control, Autom.*, **7**(2), 267-272.

Punning, A., Anton, M., Kruusmaa, M. and Aabloo, A. (2004), "A biologically inspired ray-like underwater

robot with electroactive polymer pectoral fins", *Proceedings of International IEEE Conference on Mechatronics and Robotics*, Aachen, Germany, September.

Rediniotis, O.K., Wilson, L.N., Lagoudas, D.C. and Khan, M.M. (2002), "Development of a shape-memory-alloy actuated biomimetic hydrofoil", *J. Intel. Mat. Syst. Str.*, **13**(1), 35-49.

Rossi, C., Coral W., Colorado J. and Barrientos, A. (2011), "Towards motor- less and gear less robots: a bio mimetic fish design", *Proceedings of the IEEE International Conference on Robotics and Automation*, Shanghai, China, May.

Sfakiotakis, M., Lane, D.M. and Davies, J.B.C. (1999), "Review of fish swimming modes for aquatic locomotion", *IEEE J. Oceanic Eng.*, **24**(2), 237-252.

Shahinpoor, M., Kim, K.J. and Leo, D. (2004), "Ionic polymer–metal composites as multifunctional materials", *Polym. Composite.*, **24**(1), 24-33.

Suleman, A. and Crawford, C. (2008), "Design and testing of a biomimetic tuna using shape memory alloy induced propulsion", *Comput. Struct.*, **86**(3-5), 491-499.

Technical Characteristics of Flexinol® Actuator Wires, www.dyalloy.com

Wiguna, T., Heo, S., Park, H.C. and Goo, N.S. (2009), "Design and experiment parametric study of a fish robot actuated by piezoelectric actuators", *J. Intel. Mat. Syst. Str.*, **20**(6), 751-758.

Wang, Z., Hang, G., Wang, Y., Li, J. and Du, W. (2008), "Embedded SMA wire actuated biomimetic fin: a module for biomimetic underwater propulsion", *Smart Mater. Struct.*, **17**(2), 025039, 1-11.

Wang, Z., Hang, G., Li, J., Wang, Y. and Xiao, K. (2008), "A micro-robot fish with embedded SMA wire actuated flexible biomimetic fin", *Sensor. Actuat. A. -Phys.*, **144**(2), 354-360.

Yoon, K.J., Park, K.H., Lee, S.K., Goo, N.S. and Park, H.C. (2004), "Analytical design model for a piezocomposite unimorph actuator and its verification using lightweight piezo-composite actuators", *Smart Mater. Struct.*, **13**(3), 459-467.

CC